

Highly Passivated n-Type Colloidal Quantum Dots for Solution-Processed Thermoelectric Generators with Large Output Voltage

Mohamad I. Nugraha, Hyunho Kim, Bin Sun, Saheena Desai, F. Pelayo Garcia de Arquer, Edward H. Sargent, Husam N. Alshareef, and Derya Baran*

Colloidal quantum dots (CQDs) are attractive materials for thermoelectric applications due to their simple and low-cost processing; advantageously, they also offer low thermal conductivity and high Seebeck coefficient. To date, the majority of CQD thermoelectric films reported upon have been p-type, while only a few reports are available on n-type films. High-performing n- and p-type films are essential for thermoelectric generators (TEGs) with large output voltage and power. Here, high-thermoelectric-performance n-type CQD films are reported and showcased in high-performance all-CQD TEGs. By engineering the electronic coupling in the films, a thorough removal of insulating ligands is achieved and this is combined with excellent surface trap passivation. This enables a high thermoelectric power factor of $24 \mu\text{W m}^{-1} \text{K}^{-2}$, superior to previously reported n-type lead chalcogenide CQD films operating near room temperature ($<1 \mu\text{W m}^{-1} \text{K}^{-2}$). As a result, an all-CQD film TEG with a large output voltage of 0.25 V and a power density of 0.63 W m^{-2} at $\Delta T = 50 \text{ K}$ is demonstrated, which represents an over fourfold enhancement to previously reported p-type only CQD TEGs.

Thermoelectric generators (TEGs) are devices that directly convert heat into electrical energy. These devices have drawn increased attention for their potential to harvest the dissipated heat from power plants, automotive engines, housing heating systems, and even electronic devices for micropower generation applications.^[1–5] TEGs are composed of n- and p-type semiconducting materials connected electrically in series and thermally

in parallel. The thermal-to-electrical energy conversion efficiency of the TEGs is determined by a dimensionless thermoelectric parameter of their n- and p-type constituents, $ZT = \sigma S^2 T / \kappa$, where σ , S , κ , and T are electrical conductivity, Seebeck coefficient, thermal conductivity, and absolute temperature, respectively. Recently, colloidal quantum dots (CQDs) have emerged as candidates for use in next-generation TEGs.^[6,7] This class of materials exhibits attractive thermoelectric features owing to the low dimensionality of the materials: the presence of a controllable density of grain boundaries allows for suppression of thermal conduction, enabling a strategy to increase thermoelectric performance near room temperature (RT).^[8–12] Moreover, the quantum confinement responsible for increased density of states (DOS) near the Fermi level and the carrier filtering effect are both predicted to

raise the thermoelectric conversion efficiency by increasing the Seebeck coefficient.^[13–15] CQDs have made tremendous progress as promising thermoelectric building blocks^[16–20] due to their solution processability, which allows fabrication of TEGs using cost-effective, low-temperature, and scalable printing techniques.^[21,22]


To date, CQD thermoelectrics have been reported with advanced performance approaching that of conventional bulk Bi_2Te_3 -based systems.^[16,19,23–27] However, studies on the thermoelectric properties of these materials have been limited to ingot forms requiring very high temperatures and multistep dicing processes.^[16,19,20] Film-based CQD structures offer the potential for micropower applications such as self-powered devices in sensor networks and the internet of things.^[17,28] These film-based thermoelectrics are also compatible with various coating and printing methods, simplifying upscaling and providing ease of device shaping on a broad range of substrates. While p-type films^[17,28–31] have seen rapid advancement, the thermoelectric performance of n-type counterparts still lags behind.^[32–35] High performing materials of both the p- and n-types are crucial in the fabrication of TEG devices.

In CQD films, efficient charge transport is achieved by strong inter-CQD electronic coupling through the replacement of long organic ligands with shorter ones.^[36] Unfortunately,

Dr. M. I. Nugraha, S. Desai, Prof. D. Baran
Physical Sciences and Engineering Division (PSE)
KAUST Solar Center (KSC)
King Abdullah University of Science and Technology (KAUST)
Thuwal 23955–6900, Saudi Arabia
E-mail: derya.baran@kaust.edu.sa

H. Kim, Prof. H. N. Alshareef
Physical Sciences and Engineering Division (PSE)
King Abdullah University of Science and Technology (KAUST)
Thuwal 23955–6900, Saudi Arabia

Dr. B. Sun, Dr. F. P. G. de Arquer, Prof. E. H. Sargent
Department of Electrical and Computer Engineering
University of Toronto
Toronto, Ontario M5S 3G4, Canada

 The ORCID identification number(s) for the author(s) of this article can be found under <https://doi.org/10.1002/aenm.201901244>.

DOI: 10.1002/aenm.201901244

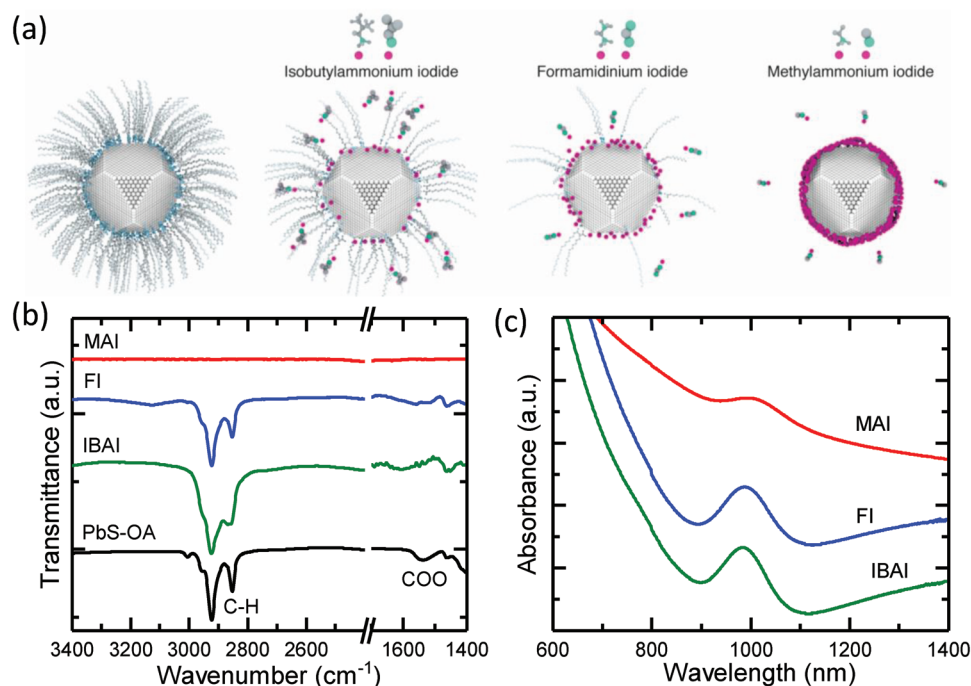


Figure 1. a) Schematic of OA ligand exchange using different iodide salts, b) FTIR, and c) optical absorption spectra of CQD films treated with different iodide salts.

incomplete exchange results in the formation of electronic trap states that, by capturing electrons during their egress through the film, suppress charge transport.^[37–40] For example, hydrazine treatments employed in the past have left the CQD surface unpassivated and disconnected, leading to poor electrical conductivity ($<10^{-2}$ S cm⁻¹) and an inefficient n-type thermoelectric power factor (<1 μ W m⁻¹ K⁻²).^[14] Prior studies have reported that halide salts could enable n-type transport in CQD thin film transistors (TFTs) and high performance solar cell devices ($\eta = 10.6\%$).^[41–49] We hypothesize that this all-inorganic halide-based ligand strategy could be deployed successfully in forming efficient n-type thermoelectrics. The halides—with their atomic size and strong affinity to cations on the CQD surface—could ultimately enhance inter-CQD electronic coupling and passivate surface defects. Thus, the use of appropriate halides in engineering the electronic coupling in films, in addition to offering excellent surface defect passivation, would be a key factor for efficient charge transport. This could lead to significant improvement of carrier mobility and density, and thus high electrical conductivity, suggesting halide-capped CQDs as promising n-type building blocks for thermoelectrics.

Here we report iodide-capped lead sulfide (PbS) CQDs as efficient solution-processed n-type thermoelectrics that allow the fabrication of all-CQD TEG devices. To engineer the electronic coupling in the CQD solids, we employ several types of iodide salts with different counterions, including isobutylammonium iodide (IBAI), formamidineum iodide (FI), and methylammonium iodide (MAI). We find that the counterions critically determine the effectiveness of oleic acid (OA) removal on the CQD surface, charge transport, and thermoelectric properties in the resulting CQD films. Given the effectiveness at OA removal and the improved trap passivation revealed by TFT

and Hall Effect studies, MAI is found to provide the most efficient charge transport and optimum doping characteristics in the CQD films. These figures of merit enable excellent n-type thermoelectrics with a power factor as high as 24 μ W m⁻¹ K⁻² at relatively low measurement temperatures (<360 K). Finally, we demonstrate an all-CQD (both p- and n-legs) TEG device with high output thermal voltage and excellent electrical power density of up to 0.25 V and 0.63 W m⁻², respectively. These values are superior to those previously reported for p-type-only CQD TEGs ($V_{\text{out}} < 50$ mV).^[14]

Figure 1a illustrates the schematic of CQDs functionalized using long aliphatic ligands. The long-alkyl-chain organic ligands provide stable colloidal dispersion in common organic solvents. In synthesis, they control the CQD size and maintain quantum confinement in the films. However, these ligands are electrically insulating that impede the inter-dot charge transport. The exchange of the long ligands with shorter ones is necessary to improve the charge transport within the CQD films. Here we selected atomic-sized monovalent iodide anions, since they have a strong affinity to the cations on the CQD surface. The negatively charged iodides readily infiltrate to the CQD surface to replace bulky OA ligands, thereby providing effective passivation of CQD surface defects, as depicted in Figure 1a. In a solid-state ligand exchange, we employed iodide anions incorporated with different counterions, including IBAI, FI, and MAI. The specific molecular sizes and unique chemical properties of the counterions are critical factors in determining the affinity of iodide anions on the CQD surface. After the ligand exchange, deprotonated OA, along with the counterions, can be rinsed away with methanol, since these were later found to be detrimental to the charge transport in the films.

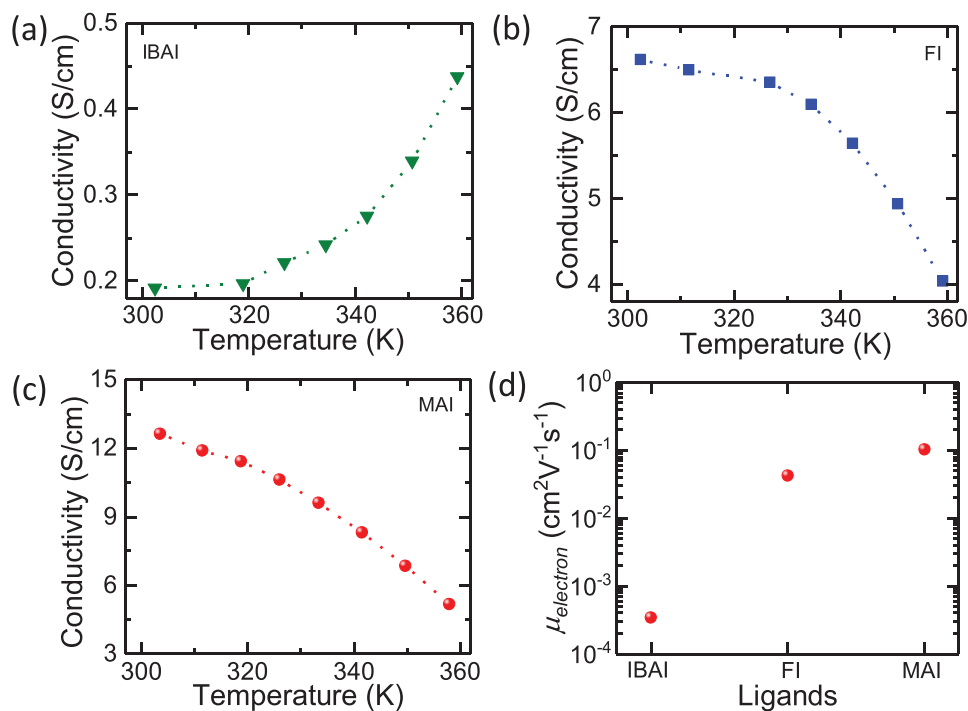


Figure 2. Temperature-dependent electrical conductivity in a) IBAI-CQD, b) FI-CQD, and c) MAI-CQD films. d) Electron mobility (μ_{electron}) extracted from TFT electrical characterization treated with different iodide salts.

Fourier transform infrared (FTIR) spectra of the CQD films treated with different iodide salts are shown in Figure 1b. The OA-CQD films exhibit C–H and COO bond stretching of around 2900 and 1500 cm^{-1} , respectively. When the CQD films are treated with IBAI (IBAI-CQDs), some C–H and COO bond stretching still appears, which reveals ineffective OA removal. The unexchanged OA ligands were found to maintain quantum confinement in the IBAI-CQD films, as validated by a sharp excitonic peak in Figure 1c. This imperfect OA removal is attributed to the increased blocking of IBAI molecules before reaching the CQD surfaces, mainly due to the larger size of the isobutylammonium counterions, as demonstrated in Figure 1a. In addition, the C–H bond stretching in the IBAI-CQD films of around 2900 cm^{-1} was also greatly enhanced, most likely due to the isobutylammonium-deprotonated OA trapped in the films even after the methanol rinse. When we treated the CQD films using smaller counterions, such as formamidinium, no significant increase in C–H bond stretching was observed, hinting at suppressed formamidinium-deprotonated OA residue in the films. In addition, the FI salts were also found to enhance the OA ligand exchange, as supported by a weaker COO bond stretching of around 1500 cm^{-1} . This result is associated with less counterion blocking as a result of smaller formamidinium size, as illustrated in Figure 1a. Despite their greater effectiveness compared to IBAI, the presence of C–H bond stretching implies some OA ligands remaining in the FI-CQD films.

We then treated the CQD films with MAI salts (MAI-CQDs) that incorporate the smallest counterion. It is clear that the C–H and COO stretching has been fully eliminated from the FTIR spectra in Figure 1b, representing complete OA removal.

The full replacement of OA ligands with atomic-sized iodide anions also enhanced inter-dot coupling, as evidenced by a broader excitonic peak in Figure 1c. Furthermore, the absence of C–H bond stretching after MAI treatment indicates that no methylammonium-deprotonated OA remained in the films. Both the clean CQD surface and the strong electronic coupling suggest the great potential of MAI to enhance charge transport and carrier density for highly conducting CQD films. To confirm that there were no structural changes in the CQD films after treatment with the iodide salts, we performed x-ray diffraction (XRD) measurements. As evidenced in Figure S1 (Supporting Information), all-CQD films exhibit three main types of facets including {111}, {200}, and {220}. A small peak around 26° was observed that corresponds to PbI_2 phase ({101}).

To investigate charge transport within the CQD films after treatment with the iodide salts, we performed four-terminal (4T) electrical conductivity measurements. Figure 2a–c displays temperature-dependent electrical conductivity in the CQD films treated with different iodide salts. The IBAI-CQD films exhibit low electrical conductivity, primarily due to incomplete OA ligand removal. We also consider that the remaining counterion-deprotonated OA plays a role in the poor electronic transport in the films, as discussed below. In particular, the unexchanged OA ligands result in larger inter-CQD spacing, preventing charge transport. This larger spacing could also be of a microscopic origin of thermally activated transport behavior in the temperature-dependent electrical conductivity (Figure 2a), as has been demonstrated previously in CQD films cross-linked with longer organic ligands.^[50] When the CQD films were treated with FI, we discovered a significant

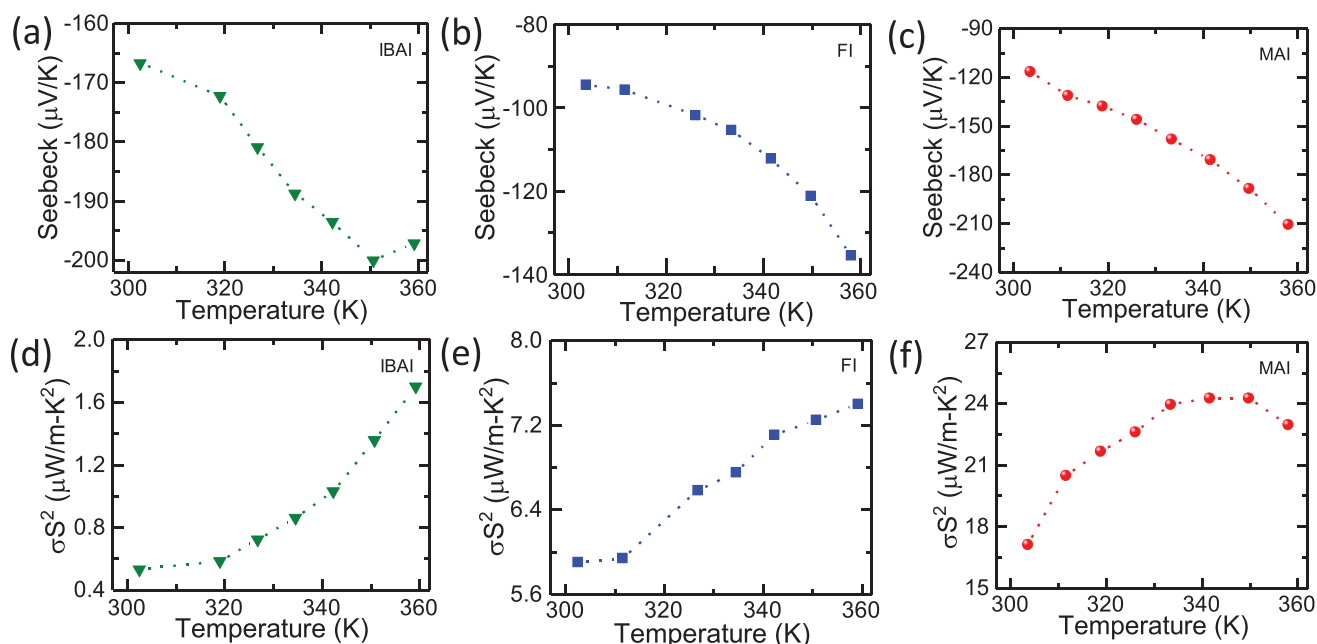


Figure 3. Temperature-dependent Seebeck coefficient and power factor in a,d) IBAI-CQD, b,e) FI-CQD, and c,f) MAI-CQD films.

increase in the electrical conductivity, as seen in Figure 2b, supporting a more complete OA replacement than that with IBAI (Figure 1b). Additionally, the suppressed density of counterion-deprotonated OA in the FI-CQD films, mentioned earlier, accounts for better charge transport, leading to improvement of more than one order of magnitude in the electrical conductivity ($\approx 6.5 \text{ S cm}^{-1}$) compared to the IBAI-CQD films.

Furthermore, an impressive improvement in electrical conductivity of 100%, exceeding 12 S cm^{-1} , was revealed in CQD films treated with MAI compared to those treated with FI, as displayed in Figure 2c. We ascribe this result both to full elimination of OA and to disadvantageous counterion-deprotonated OA excesses in the MAI-CQD films. The significant suppression of the latter may lead to reduced electron scattering induced by negatively charged deprotonated OA and thus to improved electron mean free path. The absence of positively charged counterion leftovers may also significantly minimize trapping of free electrons, enabling enhancement of electrical conductivity in the films. Furthermore, the short inter-CQD spacing in the MAI-CQD films results in the formation of continuous band-like electronic structures leading to metallic transport behavior, in contrast to the films treated with IBAI, as seen in Figure 2. Importantly, the measured electrical conductivity in the MAI-CQD films is superior to that of previously reported n-type CQD films treated with hydrazine ($<10^{-2} \text{ S cm}^{-1}$).^[14] The use of hydrazine enables thorough removal of OA; however, due to its high volatility, it leaves the CQD films disconnected and unpassivated, resulting in poor electrical conductivity.

To fully understand the 4T electrical conductivity results, we fabricated bottom-gate TFTs using CQDs treated with different iodide salts. The transfer characteristics of the SiO_2 -gated TFTs with different iodide salts are illustrated in Figure S2 (Supporting Information). It can clearly be seen that the IBAI-CQD films exhibit a noisy and low source–drain current,

while a significant improvement in the current was measured in the FI-CQD films. Additionally, subthreshold swing (SS) in the IBAI-CQD TFTs was also higher (16.6 V dec^{-1}) than in the FI-CQD TFTs (9.5 V dec^{-1}), an indication of the traps-rich nature of the former films. A further current improvement was measured in the MAI-CQD films, confirming a more favorable charge transport. The MAI-CQD films exhibited smaller SS (5.7 V dec^{-1}), which is lower by about a factor of three than that in the IBAI-CQD films. Given the SS values,^[51–53] we estimated the density of carrier traps in the MAI-CQD films to be as low as $9 \times 10^{12} \text{ cm}^{-2} \text{ eV}^{-1}$, which makes them significantly cleaner than the IBAI-CQD films ($2.6 \times 10^{13} \text{ cm}^{-2} \text{ eV}^{-1}$). The more intense charge trapping leads to poor electron mobility ($10^{-4} \text{ cm}^2 \text{ V}^{-1} \text{ s}^{-1}$) in IBAI-CQD TFTs, as presented in Figure 2d, while improvement by three orders of magnitude in the electron mobility ($0.11 \text{ cm}^2 \text{ V}^{-1} \text{ s}^{-1}$) was measured in the MAI-CQD films. With our optimized processing, the electron mobility in the MAI-CQD TFTs is significantly higher than previously reported values ($0.05 \text{ cm}^2 \text{ V}^{-1} \text{ s}^{-1}$).^[41,49] These results support our hypothesis that counterion-deprotonated OA leftovers may contribute to charge trapping, which is detrimental for electronic transport. The significant improvement in electron mobility using MAI is also supportive of the highest electrical conductivity in the films.

Figure 3a–c presents the temperature-dependent Seebeck coefficient of CQD films treated with different salts. As seen, the films using all iodide salts show negative Seebeck coefficients, which demonstrate their n-type thermoelectric behavior. These results indicate that the presence of OA ligands, with their insulating nature, does not play a significant role in the thermoelectric behavior type of CQD films, even though they are detrimental to the electrical conductivity in the films, as demonstrated in Figure 2. Near RT, the IBAI-CQD films displayed a slightly higher Seebeck coefficient than

those treated with FI and MAI, mainly due to lower electrical conductivity in the former films. Interestingly, the Seebeck coefficient of the MAI-CQD films showed the strongest temperature-dependent behavior among the CQD films, which can be attributed to a more straightforward Fermi level tuning. In n-type thermoelectrics, the Seebeck coefficient is determined by the offset between Fermi level (E_F) and conduction band (E_C), i.e., $\langle E_F - E_C \rangle$.^[10,15] Due to the more conducting nature of MAI-CQD films, increasing temperatures will easily move the Fermi level away from the conduction band, resulting in a larger Fermi–conduction band offset and thus a stronger temperature dependence of Seebeck coefficient. Meanwhile, the more insulating nature of IBAI-CQD films leads to a weaker tuning of the Fermi level–conduction band offset with temperature, leading to a smaller increase of Seebeck coefficient than in MAI-CQD films. These results elucidate another advantage of using MAI as capping ligands to enhance the Seebeck coefficient in CQD films.

The thermoelectric power factor of CQD films treated with different salts as a function of measurement temperature is represented in Figure 3d–f. The low power factor in the IBAI-CQD films derives particularly from their poor electrical conductivity. Meanwhile, a slight improvement in power factor was observed in the films treated with FI. Further power factor improvement, reaching $24 \mu\text{W m}^{-1} \text{K}^{-2}$, was measured in the MAI-CQD films. This power factor value is superior to that of previously reported n-type lead chalcogenide CQD films operating near RT ($<1 \mu\text{W m}^{-1} \text{K}^{-2}$).^[14] These results suggest a strategy for obtaining clean CQD films with strong inter-CQD coupling using MAI for efficient thermoelectric performance.

Scanning electron microscopy (SEM) measurement was performed to investigate the morphology of CQD films treated with various iodide salts (Figure 4a–c). When we used IBAI, the CQD films showed more porous structures, possibly arising from OA ligands remaining in the films. On the other hand, the FI-CQD films were less porous than IBAI-CQD films,

indicating fewer OA ligands unreplaced in the former films. The most effective OA removal, in CQD films using MAI, was found to result in a smooth and dense morphology. Atomic force microscopy (AFM) measurements were performed to support this finding. The AFM measurements in Figure 4d–f indicate that IBAI treatment results in rough and less continuous film morphology. The unexchanged OA and remaining counterion-deprotonated OA after IBAI treatment may have resulted in partially soluble films in both nonpolar and polar solvents, which are the solvents for OA- and iodide-capped CQDs, respectively. Therefore, the ensuing OA-CQD film deposition and LE process may damage the previously deposited films, resulting in rough film morphology. This effect was suppressed by treating the CQD films with FI, shown in Figure 4e. Furthermore, MAI treatment results in closely packed and smooth CQD film morphology, which is in line with the SEM results.

The most successful iodide capping, with MAI, provides excellent passivation on the CQD surface, which induces high density of free carriers and thus optimum doping concentration. To analyze the doping properties of CQD films treated with different iodide salts, we performed Hall Effect measurement. All iodide-capped CQD films were discovered to demonstrate negative Hall coefficients, which represent electrons as the majority carriers, consistent with the Seebeck measurements in Figure 3a–c. The Hall Effect carrier densities in the films treated with different iodide salts are shown in Figure 5a. Due to their more insulating nature, the IBAI-CQD films clearly exhibited low carrier density. FI- and MAI-CQD films, on the contrary, exhibited significantly higher carrier density on the order of 10^{19}cm^{-3} . These results clarify that FI and MAI treatment induces n-type doping, which is responsible for the remarkable improvement in the electrical conductivity of the films. This high carrier density supports the degenerate semiconductor properties of the FI- and MAI-CQD films, where the electrical conductivity decreases as the temperature increases, as illustrated in Figure 2b,c. Excellent defect passivation on

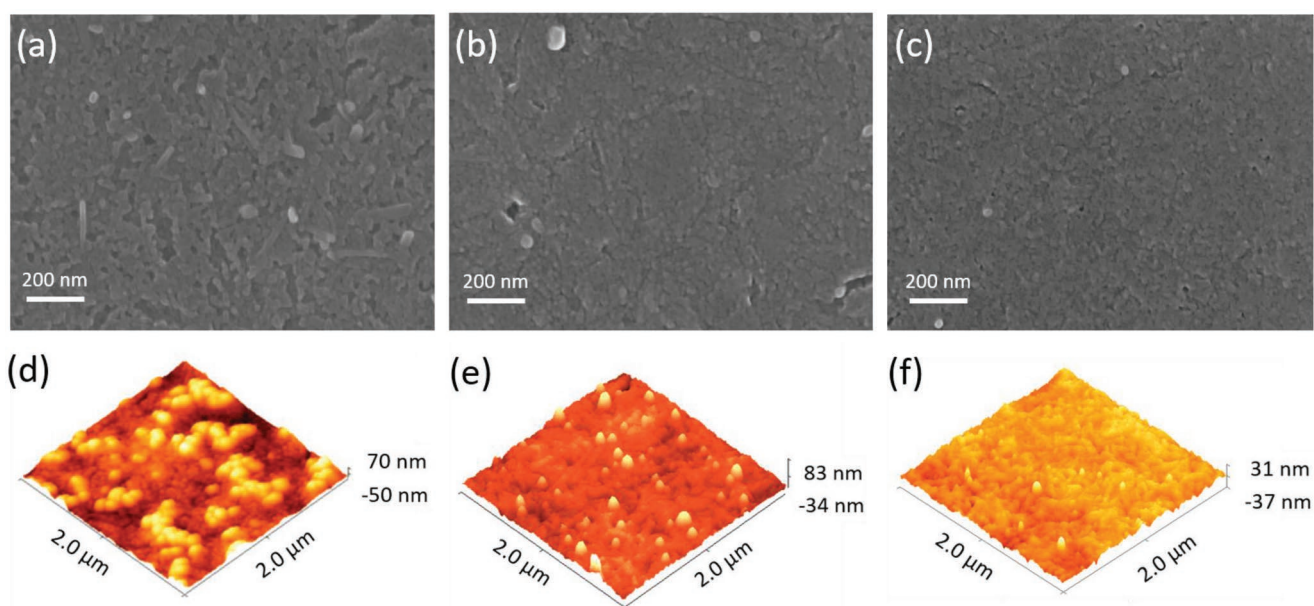


Figure 4. SEM and AFM images of a,d) IBAI-CQD, b,e) FI-CQD, and c,f) MAI-CQD films.

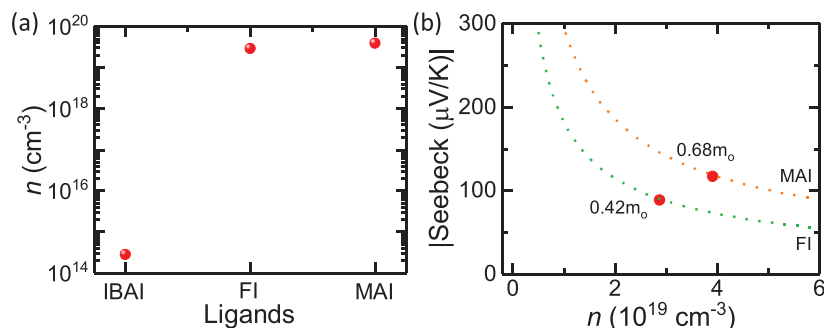


Figure 5. a) Carrier density in CQD films treated with different iodide salts. b) Electron effective mass in FI- and MAI-CQD films estimated from the Pisarenko plot.

the CQD surface results in lower trap density, leading to the highest free carrier concentration in the films with MAI. In addition, such large carrier density in the MAI-CQD films may contribute to a more straightforward Fermi level tuning, leading to a stronger temperature dependence of the Seebeck coefficient than in IBAI-CQD films.

The stronger temperature dependence of the Seebeck coefficient in MAI-CQD films implies a larger electron effective mass than that of the IBAI- and FI-CQD films. To analyze the effective mass in the films, we used the Pisarenko equation for degenerate semiconductors

$$S = \frac{8\pi^2 k_B^2}{3eh^2} m^* T \left(\frac{\pi}{3n} \right)^{2/3} (r + 1) \quad (1)$$

where n , T , k_B , e , h , m^* , and r stand for carrier density, absolute temperature, Boltzmann constant, charge constant, Planck constant, effective mass, and scattering parameter, respectively. Figure 5b presents the electron effective mass estimated from the Pisarenko plot in the FI- and MAI-CQD films. We did not quantify the electron effective mass in IBAI-CQD films using Equation (1) because of their nondegenerate semiconductor behavior. It can clearly be seen that the MAI-CQD films display greater electron effective mass than those with FI. The increased effective mass with MAI leads to the local increase of density of states (DOS), enhancing the Seebeck coefficient in the films.^[15] These results explain that the excellent defect passivation with MAI is favorable for improving electronic transport and advancing the Seebeck coefficient in the CQD films.

To demonstrate our promising n-type MAI-CQD films, we fabricated an eight p–n paired TEG. The configuration of the device is illustrated in Figure 6a. The p-type legs were constructed from CQD films treated with the ethanedithiol (EDT) ligands reported previously.^[54] The temperature-dependent Seebeck coefficient of the p-type CQD films is shown in Figure S3 (Supporting Information). In our TEG device, heat was applied from the center while the edge components of the p–n legs were left at RT. The output thermal voltage of the TEG device as a function of the temperature gradient is presented in Figure 6b. Owing to the high Seebeck coefficient of n- and p-type CQD films, we demonstrated an excellent output thermal voltage of up to 0.25 V with a temperature difference of 50 K by using eight p–n pairs. This remarkable output voltage is quite close to the estimated Seebeck coefficient

from the total number of p–n legs in the TEG device—that is, $V_T = 8(S_N + S_P)\Delta T = 8(0.12 \text{ mV K}^{-1} + 0.52 \text{ mV K}^{-1})(50 \text{ K}) = 0.26 \text{ V}$, with S_N and S_P being the Seebeck coefficients of the n- and p-type legs, respectively. We also fabricated a two p–n TEG with the output voltage shown in Figure S4 (Supporting Information). Even though we used a smaller number of p–n pairs, our two p–n TEG still displayed higher output thermal voltage than that of previously reported thin film TEG devices with more legs, due to the superior Seebeck coefficient of our CQD films.^[55–58]

Finally, the electrical power density generated by the TEG shown in Figure 6a is displayed in Figure 6c. The device delivers a power density up to $63 \mu\text{W cm}^{-2}$ (0.63 W m^{-2}) by applying a temperature gradient of 50 K. This remarkable value is the first report on the use of solution-processed PbS CQD films as both n- and p-type thermoelectric building blocks in TEG devices. These results underscore the importance of CQD systems for thermoelectric applications in the future. The output power can be improved further by enhancing the electrical conductivity of the CQD films through doping and the hybrid approach.

In conclusion, we report n-type thermoelectric properties from iodide-capped CQD films that enable the fabrication of highly efficient TEG devices. We found that the counterions in iodide salts play a critical role in the effectiveness of OA ligand removal and charge transport properties in CQD films. MAI was determined to provide efficient charge transport in the CQD films as a result of complete removal of OA ligands and excellent passivation of surface defects. These lead to a promising n-type thermoelectric power factor of up to $24 \mu\text{W m}^{-1} \text{ K}^{-2}$ at relatively low temperatures (<360 K), which represents a significant enhancement compared to previously reported n-type lead chalcogenide CQD films. The enhancement of the Seebeck coefficient in the CQD films with MAI was attributed to higher effective mass, promoting an increased DOS. Finally, the efficient n-type iodide-capped CQD leg enables the fabrication of an all-CQD film TEG demonstrating remarkable output thermal voltage and electrical power density of up to 0.25 V and 0.63 W m^{-2} , which is over four times higher than values previously reported for p-type only CQD TEGs. This study emphasizes the great importance of CQDs in realizing highly efficient next-generation TEGs for micropower applications near RT.

Experimental Section

Synthesis of PbS CQDs: CQDs were synthesized following previously reported methods.^[59] Bis(trimethylsilyl)sulfide (TMS, synthesis grade) (0.18 g, 1 mol) was added to 1-octadecene (ODE) (10 mL) that had been dried and degassed by heating to 80 °C under vacuum for 24 h. A mixture of OA (1.34 g, 4.8 mmol), PbO (0.45 g, 2.0 mmol), and ODE (14.2 g, 56.2 mmol) was heated to 95 °C under vacuum for 16 h and placed under Ar gas. The flask temperature was increased to 120 °C and the TMS/ODE mixture was injected. After injection, the flask was allowed to cool gradually to 35 °C. The CQDs were precipitated using distilled acetone (50 mL) and centrifuged. The supernatant was discarded, and the precipitate was redispersed in toluene. The CQDs were precipitated

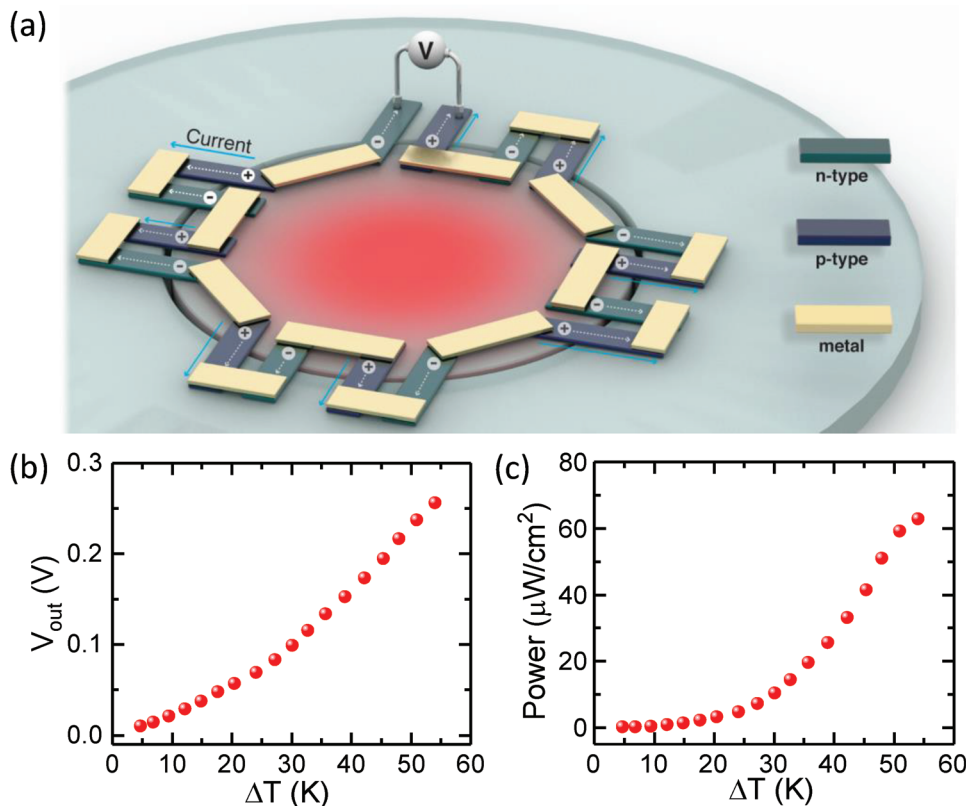


Figure 6. a) Configuration of CQD film TEG composed of eight p–n pairs. b) Output voltage and c) power density generated from eight p–n CQD film TEG as a function of the temperature gradient. The p-type legs are constructed from EDT-cross-linked CQD films.

again using methanol (20 mL), centrifuged (5 min), dried, dispersed in octane (50 mg mL⁻¹), and transported into a nitrogen glove box (oxygen below 2 ppm and moisture below 10 ppm).

Deposition of PbS CQD Films: Glass substrates were ultrasonically cleaned with acetone and isopropanol for 5 min each. After being dried at 140 °C for 10 min, the substrates were treated in a UV ozone chamber for 15 min. The solution of oleic acid-stabilized PbS CQDs in octane (50 mg mL⁻¹) was spin-coated on cleaned glass substrates. The long oleic acids were treated with iodide salts to improve charge transport within CQD films. The concentration of the iodide salts with different counterions (isobutylammonium, formamidineum, and methylammonium) was 20×10^{-3} M in methanol. The ligand exchange (LE) process was performed by dropping the iodide solution on the CQD films for 20 s, then spin-drying the solution at 2000 rpm for 60 s. Pure methanol was dropped on the films for 10 s to remove the exchanged native OA ligands. The CQD film deposition and the LE process were repeated several times to reach the desired thickness. The interlayer annealing at 200 °C for 1 min was introduced to assist removal of solvent excesses and enhance electronic coupling in each layer. Finally, the iodide-capped CQD films were annealed on a hot plate at 200 °C for 30 min.

TFT Fabrication: SiO₂/n-Si substrates with lithographically pre-patterned interdigitated Au electrodes were used. The thickness of the SiO₂ gate dielectric was 230 nm with channel length and width of 20 μm and 1 cm, respectively. The deposition of two PbS CQD thin layers and LE were performed using the above procedure. The interlayer annealing at 120 °C for 1 min was introduced to assist removal of solvent excesses and enhance electronic coupling in each layer. Finally, the iodide-capped CQD films were annealed on a hot plate at 120 °C for 30 min. All processes were performed in an N₂-filled glove box.

Fabrication of p–n TEG: The n- and p-type legs in the TEG device were constructed from PbS CQDs treated with MAI and EDT, respectively. The

EDT-cross-linked films were deposited using the previously reported procedure.^[54] Both n- and p-type films were deposited on clean glass substrates using the above method. Then, they were cut into specific size (2 cm × 1 cm) to be assembled in the TEG device. The n- and p-type legs are connected by copper wire and silver paste.

Film Characterization: The optical absorption spectra of PbS CQD films deposited on glass substrates were measured using the Cary 5000 ultraviolet–visible (UV–vis) spectrometer (Agilent Technologies). The FTIR measurements were made on films deposited on glass substrates using the Cary 680 with attenuated total reflectance (ATR) mode in air. The film thickness was measured using Tencor profilometer. XRD measurement was carried out on a Bruker D8 ADVANCE diffractometer with Cu Kα ($\lambda = 1.5406$ Å) radiation. The morphology of the CQD films was determined using SEM (Carl Zeiss Auriga). The charge carrier concentration in the films (1 cm × 1 cm on glass) was measured using the Hall Effect measurement system (Lake Shore 7700A) with the Van der Pauw configuration at RT under a magnetic field of 10 kG. The electrical characteristics of the TFT devices were measured using a Keysight B2902A precision/measure unit connected to a probe station in a glove box.

Thermoelectric Characteristic Measurement: Electrical conductivity and Seebeck coefficient were measured by the linear four-probe and temperature differential methods, respectively. The measurement was performed using thermoelectric characterization setup RZ2001i (Ozawa Science Co. Ltd., Japan) under a continuous flow of Ar/H₂ gas. The output voltage (V) of the p–n TEG was recorded using a Fluke 87 V multimeter in a glove box. The output electrical power (P) was calculated by measuring the total internal electrical resistance of the p–n arrays (R) and using the equation $P = V^2/R$. The heat on the hot side of the TEG was applied using Peltier devices, while the edge components of the p–n legs were left at RT. The temperatures of both hot and cold sides were probed using K-type thermocouples.

Supporting Information

Supporting Information is available from the Wiley Online Library or from the author.

Acknowledgements

The authors would like to acknowledge Xinwei Guan for supporting XRD measurement. Figures 1a and 6a were created by Heno Hwang, a scientific illustrator at King Abdullah University of Science and Technology (KAUST). This publication is based upon work supported by the King Abdullah University of Science and Technology (KAUST) Office of Sponsored Research (OSR) under Award No. OSR-CRG2018-3737.

Conflict of Interest

The authors declare no conflict of interest.

Keywords

colloidal quantum dots, ligands, n-type thermoelectrics, solution-processed semiconductors, thermoelectric generators

Received: April 17, 2019

Revised: May 29, 2019

Published online:

- [1] D. Zhao, S. Fabiano, M. Berggren, X. Crispin, *Nat. Commun.* **2017**, *8*, 1.
- [2] Y. Chen, Y. Zhao, Z. Liang, *Energy Environ. Sci.* **2015**, *8*, 401.
- [3] O. Bubnova, X. Crispin, *Energy Environ. Sci.* **2012**, *5*, 9345.
- [4] Y. Liu, G. García, S. Ortega, D. Cadavid, P. Palacios, J. Lu, M. Ibáñez, L. Xi, J. De Roo, A. M. López, S. Martí-Sánchez, I. Cabezas, M. de la Mata, Z. Luo, C. Dun, O. Dobrozhan, D. L. Carroll, W. Zhang, J. Martins, M. V. Kovalenko, J. Arbiol, G. Noriega, J. Song, P. Wahnón, A. Cabot, *J. Mater. Chem. A* **2017**, *5*, 2592.
- [5] B. Russ, A. Glauddell, J. J. Urban, M. L. Chabiny, R. A. Segalman, *Nat. Rev. Mater.* **2016**, *1*, 16050.
- [6] J. Choi, K. Cho, J. Yun, Y. Park, S. Yang, S. Kim, *Adv. Energy Mater.* **2017**, *7*, 1.
- [7] J. J. Urban, *Nat. Nanotechnol.* **2015**, *10*, 997.
- [8] C. J. Vineis, A. Shakouri, A. Majumdar, M. G. Kanatzidis, *Adv. Mater.* **2010**, *22*, 3970.
- [9] A. Muto, A. Minnich, B. Poudel, B. Yu, D. Vashaee, D. Wang, G. Chen, J. Liu, M. S. Dresselhaus, Q. Hao, X. Yan, X. Chen, Y. Ma, Y. Lan, Z. Ren, *Science* **2008**, *320*, 634.
- [10] M. S. Dresselhaus, G. Chen, M. Y. Tang, R. Yang, H. Lee, D. Wang, Z. Ren, J. P. Fleurial, P. Gogna, *Adv. Mater.* **2007**, *19*, 1043.
- [11] M. G. Kanatzidis, *Chem. Mater.* **2010**, *22*, 648.
- [12] A. I. Hochbaum, R. Chen, R. D. Delgado, W. Liang, E. C. Garnett, M. Najarian, A. Majumdar, P. Yang, *Nature* **2008**, *451*, 163.
- [13] D. Yang, C. Lu, H. Yin, I. P. Herman, *Nanoscale* **2013**, *5*, 7290.
- [14] R. Y. Wang, J. P. Feser, J. S. Lee, D. V. Talapin, R. Segalman, A. Majumdar, *Nano Lett.* **2008**, *8*, 2283.
- [15] G. J. S. Joseph, P. Heremans, V. Jovic, E. S. Toberer, A. Saramat, K. Kurosaki, A. Charoenphakdee, S. Yamanaka, *Science* **2008**, *321*, 554.
- [16] S. Ortega, M. Ibáñez, Y. Liu, Y. Zhang, M. V. Kovalenko, D. Cadavid, A. Cabot, *Chem. Soc. Rev.* **2017**, *46*, 3510.
- [17] D. Ding, D. Wang, M. Zhao, J. Lv, H. Jiang, C. Lu, Z. Tang, *Adv. Mater.* **2017**, *29*, 1603444.
- [18] D. H. Gu, S. Jo, H. Jeong, H. W. Ban, S. H. Park, S. H. Heo, F. Kim, J. I. Jang, J. E. Lee, J. S. Son, *ACS Appl. Mater. Interfaces* **2017**, *9*, 19143.
- [19] M. Ibáñez, Z. Luo, A. Genç, L. Piveteau, S. Ortega, D. Cadavid, O. Dobrozhan, Y. Liu, M. Nachtegaal, M. Zebarjadi, J. Arbiol, M. V. Kovalenko, A. Cabot, *Nat. Commun.* **2016**, *7*, 1.
- [20] M. Ibáñez, R. Zamani, S. Gorsse, J. Fan, S. Ortega, D. Cadavid, J. R. Morante, J. Arbiol, A. Cabot, *ACS Nano* **2013**, *7*, 2573.
- [21] C. Han, G. Tan, T. Varghese, M. G. Kanatzidis, Y. Zhang, *ACS Energy Lett.* **2018**, *3*, 818.
- [22] L. Wang, Z. Zhang, L. Geng, T. Yuan, Y. Liu, J. Guo, L. Fang, J. Qiu, S. Wang, *Energy Environ. Sci.* **2018**, *11*, 1307.
- [23] M. V. Kovalenko, M. I. Bodnarchuk, J. Zaumseil, J.-S. Lee, D. V. Talapin, *J. Am. Chem. Soc.* **2010**, *132*, 10085.
- [24] J. D. Forster, J. J. Lynch, N. E. Coates, J. Liu, H. Jang, E. Zaia, M. P. Gordon, M. Szybowski, A. Sahu, D. G. Cahill, J. J. Urban, *Sci. Rep.* **2017**, *7*, 1.
- [25] C. Zhou, Y. K. Lee, J. Cha, B. Yoo, S. P. Cho, T. Hyeon, I. Chung, *J. Am. Chem. Soc.* **2018**, *140*, 9282.
- [26] H. Zhang, J. S. Son, D. S. Dolzhenkov, A. S. Filatov, A. Hazarika, Y. Wang, M. H. Hudson, C. J. Sun, S. Chattopadhyay, D. V. Talapin, *Chem. Mater.* **2017**, *29*, 6396.
- [27] K. Biswas, J. He, I. D. Blum, C. I. Wu, T. P. Hogan, D. N. Seidman, V. P. Dravid, M. G. Kanatzidis, *Nature* **2012**, *489*, 414.
- [28] S. Jo, S. Choo, F. Kim, S. H. Heo, J. S. Son, *Adv. Mater.* **2018**, *31*, 1804930.
- [29] J. Luo, D. Billep, T. Waechter, T. Otto, M. Toader, O. Gordan, E. Sheremet, J. Martin, M. Hietschold, D. R. T. Zahn, T. Gessner, *J. Mater. Chem. A* **2013**, *1*, 7576.
- [30] E. Lim, K. A. Peterson, G. M. Su, M. L. Chabiny, *Chem. Mater.* **2018**, *30*, 998.
- [31] H. Liu, X. Shi, F. Xu, L. Zhang, W. Zhang, L. Chen, Q. Li, C. Uher, T. Day, G. J. Snyder, *Nat. Mater.* **2012**, *11*, 422.
- [32] D. Yoo, J. J. Lee, C. Park, H. H. Choi, J.-H. Kim, *RSC Adv.* **2016**, *6*, 37130.
- [33] S. Wang, H. Sun, T. Erdmann, G. Wang, D. Fazzi, U. Lappan, Y. Puttisong, Z. Chen, M. Berggren, X. Crispin, A. Kiri, B. Voit, T. J. Marks, S. Fabiano, A. Facchetti, *Adv. Mater.* **2018**, *30*, 1801898.
- [34] S. Wang, H. Sun, U. Ail, M. Vagin, P. O. Å. Persson, J. W. Andreasen, W. Thiel, M. Berggren, X. Crispin, D. Fazzi, S. Fabiano, *Adv. Mater.* **2016**, *28*, 10764.
- [35] P. L. Miller, E. E. Perry, R. A. Segalman, M. L. Chabiny, B. Russ, F. G. Brunetti, W. B. Chang, M. J. Robb, V. Ho, J. J. Urban, S. N. Patel, C. J. Hawker, *Adv. Mater.* **2014**, *26*, 3473.
- [36] M. I. Nugraha, H. Matsui, S. Watanabe, T. Kubo, R. Häusermann, S. Z. Bisri, M. Sytnyk, W. Heiss, M. A. Loi, J. Takeya, *Adv. Electron. Mater.* **2017**, *3*, 1600360.
- [37] S. J. Oh, N. E. Berry, J.-H. Choi, E. A. Gaulding, H. Lin, T. Paik, B. T. Diroll, S. Muramoto, C. B. Murray, C. R. Kagan, *Nano Lett.* **2014**, *14*, 1559.
- [38] D. V. Talapin, J.-S. Lee, M. V. Kovalenko, E. V. Shevchenko, *Chem. Rev.* **2010**, *110*, 389.
- [39] Z. Ning, O. Voznyy, J. Pan, S. Hoogland, V. Adinolfi, J. Xu, M. Li, A. R. Kirmani, J. Sun, J. Minor, K. W. Kemp, H. Dong, L. Rollny, A. Labelle, G. Carey, B. Sutherland, I. Hill, A. Amassian, H. Liu, J. Tang, O. M. Bakr, E. H. Sargent, *Nat. Mater.* **2014**, *13*, 822.
- [40] S. J. Oh, D. B. Straus, T. Zhao, J.-H. Choi, S.-W. Lee, E. A. Gaulding, C. B. Murray, C. R. Kagan, *Chem. Commun.* **2017**, *53*, 728.
- [41] M. I. Nugraha, S. Kumagai, S. Watanabe, M. Sytnyk, W. Heiss, M. A. Loi, J. Takeya, *ACS Appl. Mater. Interfaces* **2017**, *9*, 18039.
- [42] X. Lan, O. Voznyy, A. Kiani, F. P. García De Arquer, A. S. Abbas, G. H. Kim, M. Liu, Z. Yang, G. Walters, J. Xu, M. Yuan, Z. Ning, F. Fan, P. Kanjanaboos, I. Kramer, D. Zhitomirsky, P. Lee, A. Perelgut, S. Hoogland, E. H. Sargent, *Adv. Mater.* **2016**, *28*, 299.

- [43] D. J. Milliron, *Nat. Mater.* **2014**, *13*, 772.
- [44] C. M. Chuang, P. R. Brown, V. Bulović, M. G. Bawendi, *Nat. Mater.* **2014**, *13*, 796.
- [45] D. Zhitomirsky, M. Furukawa, J. Tang, P. Stadler, S. Hoogland, O. Voznyy, H. Liu, E. H. Sargent, *Adv. Mater.* **2012**, *24*, 6181.
- [46] J. Tang, K. W. Kemp, S. Hoogland, K. S. Jeong, H. Liu, L. Levina, M. Furukawa, X. Wang, R. Debnath, D. Cha, K. W. Chou, A. Fischer, A. Amassian, J. B. Asbury, E. H. Sargent, *Nat. Mater.* **2011**, *10*, 765.
- [47] L. Han, D. M. Balazs, A. G. Shulga, M. Abdu-Aguye, W. Ma, M. A. Loi, *Adv. Electron. Mater.* **2018**, *4*, 1.
- [48] X. Lan, O. Voznyy, F. P. García De Arquer, M. Liu, J. Xu, A. H. Proppe, G. Walters, F. Fan, H. Tan, M. Liu, Z. Yang, S. Hoogland, E. H. Sargent, *Nano Lett.* **2016**, *16*, 4630.
- [49] D. M. Balazs, D. N. Dirin, H. H. Fang, L. Protesescu, G. H. Ten Brink, B. J. Kooi, M. V. Kovalenko, M. A. Loi, *ACS Nano* **2015**, *9*, 11951.
- [50] K. Szendrei, M. Speirs, W. Gomulya, D. Jarzab, M. Manca, O. V. Mikhnenko, M. Yarema, B. J. Kooi, W. Heiss, M. A. Loi, *Adv. Funct. Mater.* **2012**, *22*, 1598.
- [51] M. I. Nugraha, R. Häusermann, S. Watanabe, H. Matsui, M. Sytnyk, W. Heiss, J. Takeya, M. A. Loi, *ACS Appl. Mater. Interfaces* **2017**, *9*, 4719.
- [52] M. I. Nugraha, R. Häusermann, S. Z. Bisri, H. Matsui, M. Sytnyk, W. Heiss, J. Takeya, M. A. Loi, *Adv. Mater.* **2015**, *27*, 2107.
- [53] M. I. Nugraha, H. Matsui, S. Z. Bisri, M. Sytnyk, W. Heiss, M. A. Loi, J. Takeya, *APL Mater.* **2016**, *4*, 116105.
- [54] M. I. Nugraha, H. Kim, B. Sun, M. A. Haque, F. P. G. de Arquer, D. R. Villalva, A. El-Labban, E. H. Sargent, H. N. Alshareef, D. Baran, *Adv. Energy Mater.* **2019**, *9*, 1803049.
- [55] X. Wang, F. Meng, T. Wang, C. Li, H. Tang, Z. Gao, S. Li, F. Jiang, J. Xu, *J. Alloys Compd.* **2018**, *734*, 121.
- [56] J. J. Lee, D. Yoo, C. Park, H. H. Choi, J. H. Kim, *Sol. Energy* **2016**, *134*, 479.
- [57] E. Jin Bae, Y. Hun Kang, K. S. Jang, S. Yun Cho, *Sci. Rep.* **2016**, *6*, 1.
- [58] E. J. Bae, Y. H. Kang, K. S. Jang, C. Lee, S. Y. Cho, *Nanoscale* **2016**, *8*, 10885.
- [59] M. A. Hines, G. D. Scholes, *Adv. Mater.* **2003**, *15*, 1844.